Hindawi
Geofluids
Volume 2022, Article ID 8101861, 11 pages
https://doi.org/10.1155/2022/8101861

Research Article

Time-Frequency Characteristics of Acoustic Emission Signals on Water-Bearing Sandstone Specimen Subjected to Conventional Uniaxial Compression

Hui-qiang Duan,[1] **Ming-tao Gao**,[2,3] **and Hong-yu Yan**[3]

[1]*School of Mining and Coal, Inner Mongolia University of Science and Technology, Baotou 014010, China*
[2]*College of Energy and Mining Engineering, Shandong University of Science and Technology, Qingdao 266590, China*
[3]*School of Emergency Technology and Management, North China Institute of Science & Technology, Langfang 065201, China*

Correspondence should be addressed to Ming-tao Gao; gmthww@163.com

Received 5 January 2022; Accepted 6 April 2022; Published 11 May 2022

Academic Editor: Andrea Brogi

This paper presents an experimental investigation of acoustic emission (AE) time-frequency characteristics of a water-bearing sandstone specimen in a conventional uniaxial compression test. The main achievements are as follows: (1) The violent fluctuation of AE time domain parameters indicates that the water-bearing sandstone specimen is about to be destroyed. This characteristic provides a theoretical basis for predicting the failure of water-bearing rock in engineering practice. (2) In the elastic phase, the AE *b* value is the lowest but has a sudden increase after falling into the steady crack propagation phase. In the unsteady crack propagation phase, the AE *b* value is further increased. This characteristic is of great indicative value for predicting the failure of the water-bearing sandstone specimen. (3) The difference of dominant frequency among the three key points is very small, indicating that the crack initiation and propagation of the water-bearing sandstone specimen has a certain stability in the damage and failure process. But, the two-dimensional frequency spectrum structure of AE waveform signals shows that the closer to failure, the more the number of the frequency spectrum structure peaks. (4) The energy of AE signals is mainly concentrated in the first three frequency bands. The closer to failure, the more the energy proportion of the first three frequency bands is reduced; conversely, the energy proportion of the latter five frequency bands is increased, which leads to more complexity of the failure modes of the water-bearing sandstone specimen.

1. Introduction

Deep mining is not only affected by the high ground stress and high gas pressure but also affected by the high karst water pressure; under the physical and chemical actions of water, the rock composition and structure will change at the fine and microlevel, thus resulting in more complex mechanical behavior [1–4]. In China, many serious mine water-inrush accidents have happened, such as the water-inrush accidents in the Yongsheng coal mine on July 7, 2019, in the Wangjialing coal mine on March 28, 2010, and in the Daxing coal mine on August 7, 2005. These accidents have caused serious heavy losses of life and property. So, it is of great significance for the safe and efficient production of coal mine to carry out the mechanical test of water-bearing rock and study its precursory characteristics of failure. Now, there are many studies on the strength characteristics of water-bearing rocks, and a consistent conclusion has been reached, namely, that the strength of rocks is inversely proportional to the moisture content. However, the strength index cannot be used as a precursor parameter for predicting the water-bearing rock failure, because it only reflects the strength value at failure. In order to determine the reasonable precursory parameters of water-bearing rock failure, it is necessary to deeply analyze its AE characteristics. As we all know, in the damage and failure process of loaded rock, the rock microcracks continue to generate and release strain energy in the form of an elastic wave, which is the AE

phenomenon [5–9]. The AE signals contain rich information about the development and evolution of the rock internal fracture, which is an important manifestation form of rock deformation and failure [10–14]. Therefore, to further study the rock AE characteristics can effectively evaluate the damage state of the rock, and it also has an important theoretical guiding significance for predicting and preventing rock instability disasters. The analysis of AE signals is mainly divided into two methods, namely, the time domain parameter analysis and the frequency domain waveform analysis [15]. The time domain parameter analysis can only reveal some eigenvalue changes in the process of rock failure. However, the frequency domain waveform analysis can deeply mine the rich information contained in the AE waveform signals, and the extracted spectrum features can more comprehensively reflect the rock failure mechanism [16].

At present, some achievements have been made in the frequency domain analysis of rock AE waveform signals. For example, Li et al. [17] studied the AE waveform characteristics of rock mass under uniaxial loading. Du et al. [18] studied the time-frequency characteristics of tensile and shear cracks of rock in various types of tests. Sheng et al. [19] studied the frequency characteristics of various AE signals during high-velocity waterjet rock drilling. Mei et al. [20] studied the main frequency precursor characteristics of AE signals from deeply buried Dali rock explosion. Zeng et al. [21] proposed a dominant frequency identification criterion model of multiband AE signals based on the relationship between AE signal frequency band proportion and rock stress through the uniaxial compression AE test of gritstone, which has certain theoretical significance for the prediction of rock instability and failure. He et al. [22] studied the evolution law of AE spectrum characteristics of granite through an instantaneous strain rockburst simulation test and obtained the dominant frequency and the evolution characteristics of a two-dimensional spectrum of AE signals under different stress values.

However, most of the current studies are related to dry specimens, and the research on the spectrum characteristics of AE signals of water-bearing rock is relatively rare. Based on this, this paper firstly obtains the original AE waveform signals of the water-bearing sandstone specimen through the conventional uniaxial compression test, then denoises these signals, obtains the two-dimensional spectrum by the fast Fourier transform (FFT), and extracts the dominant frequency. At the same time, the wavelet packet analysis is used to study the energy distribution characteristics of AE signals in different frequency bands.

2. Specimens and Experimental Devices

2.1. Specimens. The sandstone samples were from the Yangcun Coal Mine in Shandong, China. These samples were processed into several standard cylindrical specimens with a diameter of 50 mm and a height of 100 mm. The basic information of specimens are listed in Table 1.

Table 1: The basic information of water-bearing sandstone specimen.

Specimen number	Diameter (mm)	Height (mm)	Mass (g)
S1	49.44	99.96	426.3
S2	49.50	99.82	428.2
S3	49.52	98.56	424.6
S4	49.46	99.78	429.1

Figure 1: MTS815.02 rock mechanics test system.

2.2. Experimental Device and Method. A conventional uniaxial compression test is conducted using the MTS815.02 rock mechanics test system (MTS Systems Corporation, Eden Prairie, MN, USA) from the China University of Mining and Technology, as shown in Figure 1. Prior to each test, these specimens were firstly subjected to the immersion test for 24 hours; then, an initial force of 1.0 kN was applied to each water-bearing sandstone specimen to ensure close contact between the test machine pressure head and the specimen. The displacement control mode with a loading rate of 0.003 mm/s was employed. In order to ensure the safety of the test machine, it is set that the test is over when the axial displacement of these specimens exceeds 3 mm. The AE21C AE system (Shenyang Computer Technology Research and Design Institute, Shenyang, China) is employed. The sampling frequency is set to be 1.0 MHz. The preamplifier gain and threshold were set to be 36.0 and 30.0 dB, respectively. The MTS815.02 test system and AE21C AE system were operated simultaneously during the tests.

3. Test Results and Analysis

3.1. AE Characteristics in Time Domain

3.1.1. AE Ring Count Rate. Limited by space, the AE data of the no. S1 water-bearing sandstone specimen is selected for studying and analysis. Figure 2 shows the corresponding AE ring count rate and axial stress versus time curve. The evolution process of the AE ring count rate can be divided into four phases, namely, the slow growth, rapid growth, steady fluctuation, and violent fluctuation phases. In the slow growth phase, the AE ring count rate does not exceed 2600/s, which is roughly corresponding to the compaction phase and the early term of the elastic phase

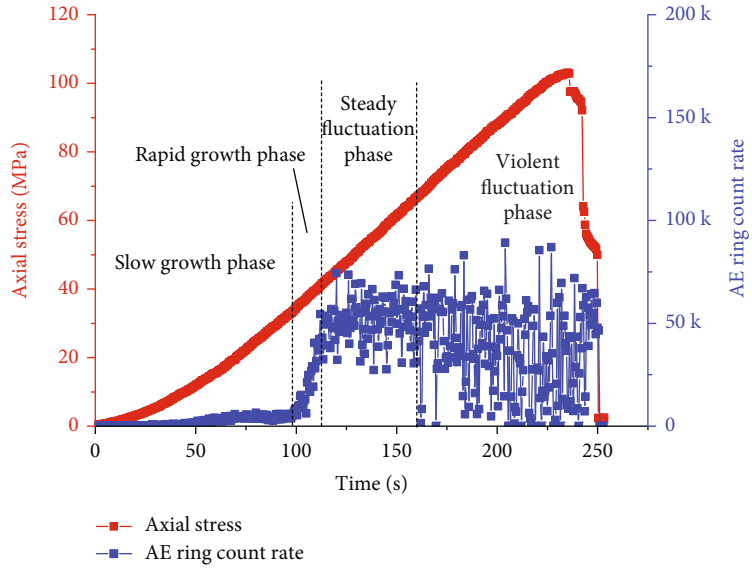

Figure 2: AE ring count rate and axial stress versus time curve.

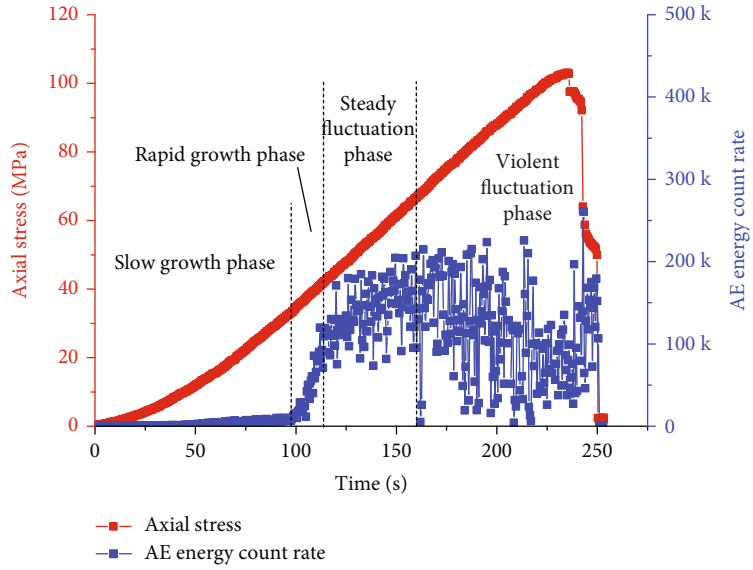

Figure 3: AE energy count rate and axial stress versus time curve.

of the water-bearing sandstone specimen. In this phase, the water-bearing sandstone specimen is mainly compacted by microcracks, and it basically generates no new cracks. In the rapid growth phase, the AE ring count rate basically increases linearly, indicating that the microcracks in the water-bearing sandstone specimen initiate at some stable rate, which is roughly corresponding to the midterm of the elastic phase of the water-bearing sandstone specimen. In the steady fluctuation phase, the AE ring count rate fluctuates from 25000/s to 75000/s, which is roughly corresponding to the later term of the elastic phase of the water-bearing sandstone specimen. In the violent fluctuation phase, the AE ring count rate fluctuates from 0 to 90000/s, and the fluctuation range is further expanded, corresponding to the unsteady crack propagation and failure phase of the water-bearing sandstone.

3.1.2. AE Energy Count Rate. Figure 3 shows the AE energy count rate and axial stress versus time curve. The evolution process of the AE energy count rate can be divided into four phases, namely, the slow growth, rapid growth, steady fluctuation, and violent fluctuation phases. By comparing Figure 2 with Figure 3, it can be seen that the four-phase division of the AE energy count rate is in line with the ring count rate.

3.1.3. AE Hit Count Rate. Figure 4 shows the AE hit count rate and axial stress versus time curve. The evolution process

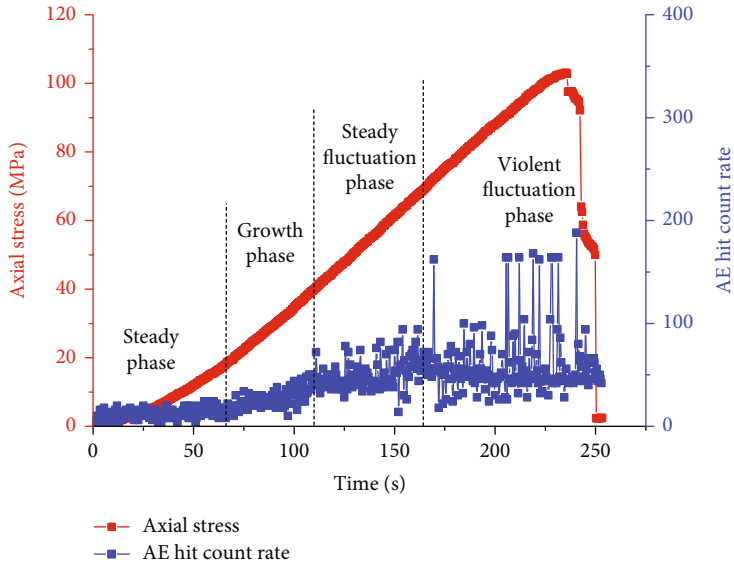

Figure 4: AE hit count rate and axial stress versus time curve.

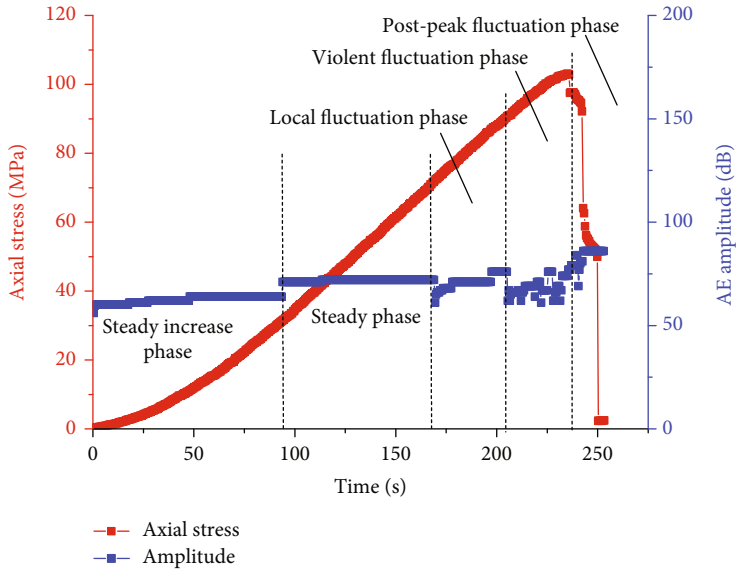

Figure 5: AE amplitude and axial stress versus time curve.

of the AE hit count rate can be divided into four phases, namely, the steady, growth, steady fluctuation, and violent fluctuation phases. In the steady phase, the AE hit count rate keeps basically stable, which is roughly corresponding to the compaction phase of the water-bearing sandstone specimen. In the growth phase, the AE hit count rate basically increases linearly, which is roughly corresponding to the early term of the elastic phase of the water-bearing sandstone specimen. In the steady fluctuation phase, the AE hit count rate fluctuates from 10/s to 100/s, which is roughly corresponding to the later term of the elastic phase of the water-bearing sandstone specimen. In the violent fluctuation phase, the AE hit count rate fluctuates from 20/s to 200/s and the fluctuation range is further expanded. Besides, a large count rate appears every some time interval. This phase is corresponding to the unsteady crack propagation and failure phase of the water-bearing sandstone.

3.1.4. AE Amplitude and b Value. Figure 5 shows the AE amplitude and axial stress versus time curve. The evolution process of the AE amplitude can be divided into five phases, namely, the steady increase, steady, local fluctuation, violent fluctuation, and postpeak fluctuation phases. The violent fluctuation phase is corresponding to the unsteady crack growth, and its occurrence can be regarded as the precursory characteristics of water-bearing sandstone specimen failure.

The AE *b* value comes from seismology. Through the study of global earthquake activities, Gutenberg and Richter

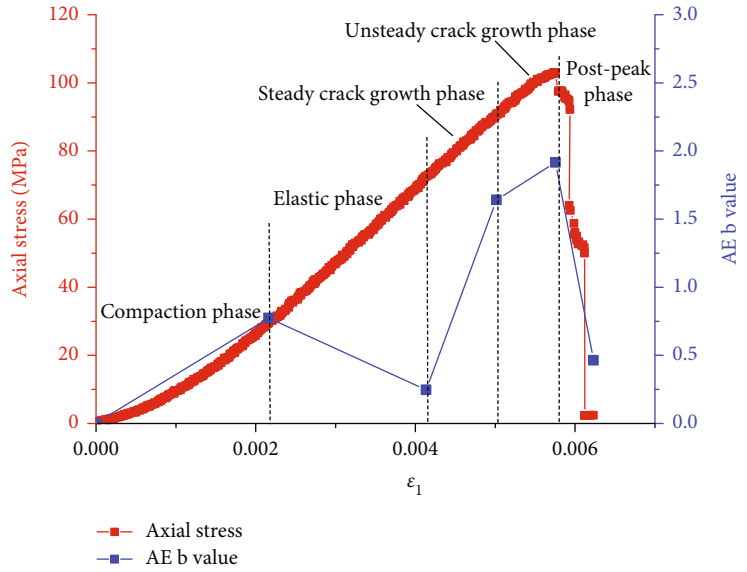

Figure 6: AE b value evolution curve. The symbol ε_1 is the axial strain.

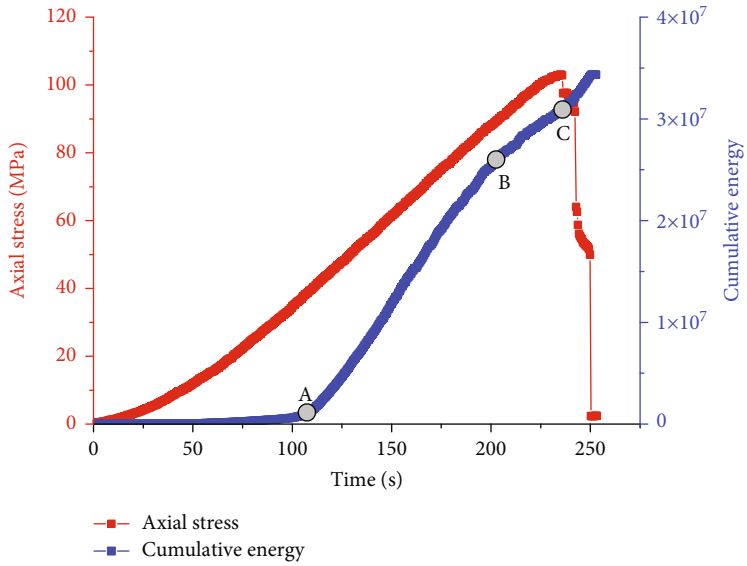

Figure 7: Key point selection based on AE cumulative energy.

put forward the G-R relationship between earthquake magnitude and occurrence times, with the relationship equation as follows [23]:

$$\lg N = a - bM, \tag{1}$$

where M is the earthquake magnitude, N is the number of earthquakes with the magnitude greater than or equal to M, and a and b are the constants.

The AE activities in the rock mechanics test also belong to the vibration, which has the same physical meaning as earthquake activities. But, there exists no concept of the magnitude in the rock AE test. Therefore, it is necessary to turn the AE amplitude into the equivalent magnitude. The following equation is generally used [23]:

$$M_L = \frac{M_s}{20}, \tag{2}$$

where M_s is the AE amplitude during the lab test and M_L is the equivalent magnitude during the lab test.

So, the G-R relationship in rock AE research is as follows:

$$\lg N = a - bM_L. \tag{3}$$

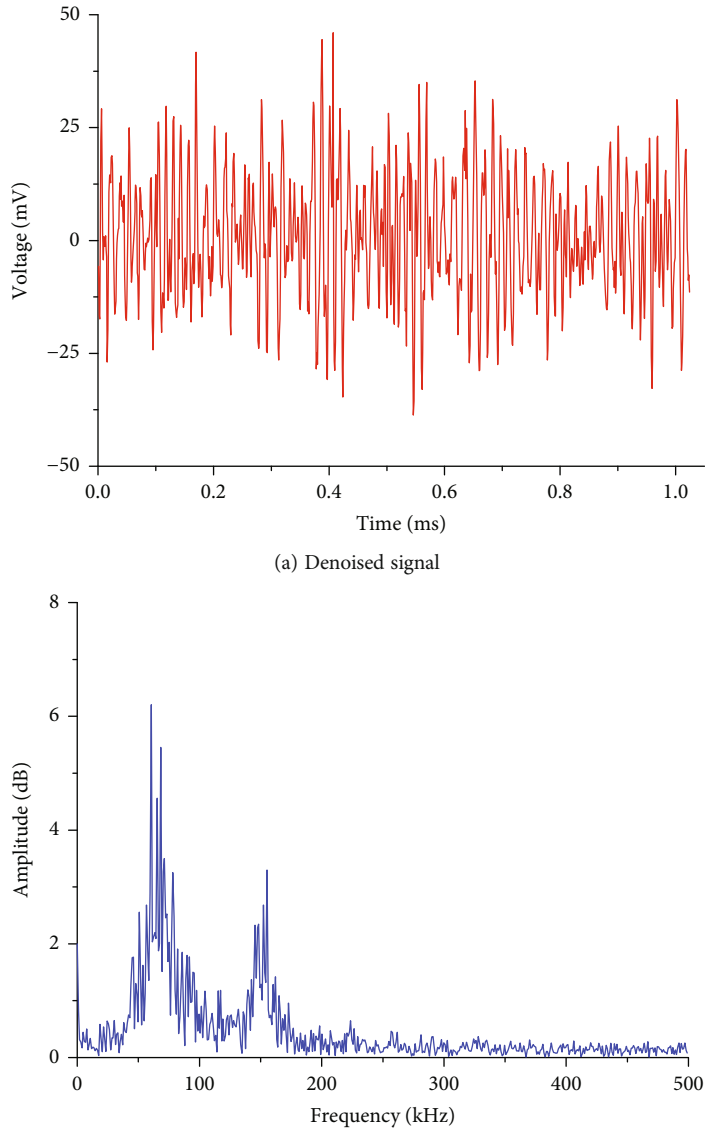

(a) Denoised signal

(b) Two-dimensional frequency spectrum

Figure 8: Denoised signals and two-dimensional frequency spectrum near key point "A.".

Table 2: The AE *b* value in different phases.

Phase	Compaction	Elasticity	Steady crack growth	Unsteady crack growth	Postpeak
AE *b* value	0.7732	0.2469	1.6414	1.9164	0.4629

Because the stress-strain curve can be divided into five phases, namely, compaction, elastic, steady crack growth, unsteady crack growth, and postpeak phases, so the AE amplitude in the five phases is firstly turned into the equivalent magnitude according to Equation (2). Then, these data are summarized and analyzed according to the magnitude interval of 0.05 dB to obtain the earthquake frequency. Finally, the AE *b* value is obtained by Equation.(3).

Table 2 and Figure 6 shows the evolution curve of the AE *b* value of the water-bearing sandstone specimen in different phases. From Table 2 and Figure 6, the AE *b* value in the elastic phase is the lowest, but the AE *b* value has a sudden increase after falling into the steady crack growth phase. In the unsteady crack growth phase, the AE *b* value is further increased. This characteristic is of great indicative value for predicting the failure of the water-bearing sandstone specimen.

3.1.5. Discussions. By comparing Figure 2 with Figure 4, it can be seen that there are some differences in the four-phase division of the AE ring count rate and hit count rate; they are consistent only in the latter two phases. Before the failure of the water-bearing sandstone specimen, the AE time domain parameters, including the AE ring count rate,

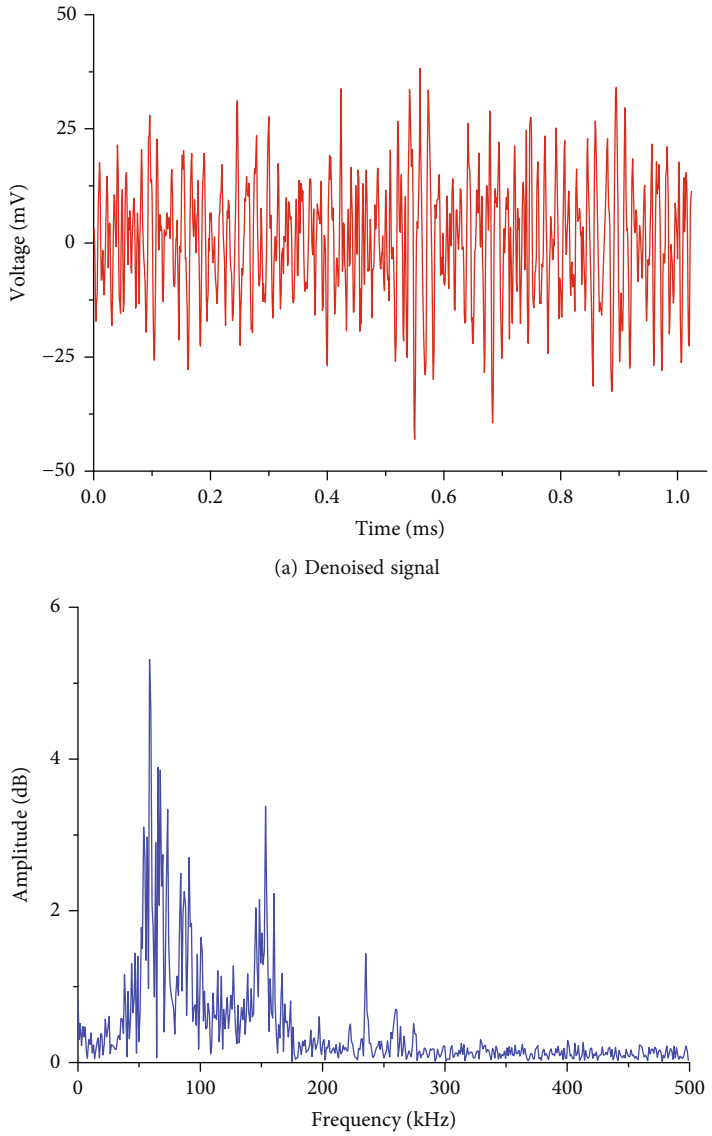

(a) Denoised signal

(b) Two-dimensional frequency spectrum

Figure 9: Denoised signals and two-dimensional frequency spectrum near key point "B.".

energy count rate, hit count rate, and amplitude, show the violent fluctuation characteristics. So, the violent fluctuation of AE time domain parameters indicates that the water-bearing sandstone specimen is about to be destroyed. This characteristic provides a theoretical basis for predicting the failure of water-bearing rock in engineering practice. The AE hit count rate reflects the frequency of crack propagation, so the failure of the water-bearing sandstone specimen should be measured by the AE hit count rate. From Figure 4, the maximum value of the AE hit count rate occurs after the peak stress. This shows that the water-bearing sandstone specimen will be destroyed at some time point after the postpeak phase.

3.2. AE Characteristics in Frequency Domain

3.2.1. Key Point Selection. The research shows that the compression failure of rock is a process of energy absorption and release, and the AE energy reflects the released elastic energy during the initiation or propagation of cracks in rock. Therefore, in-depth study of the AE energy characteristics is helpful to reveal the essential characteristics of AE activities. Due to the large number of AE signals in the test process, several representative key points need to be chosen for analysis. The selection principle of key points is the turning point with obvious change in the AE cumulative energy curve.

As shown in Figure 7, three key points are chosen. The key point "A" is the inflection point from slow growth to rapid growth in the cumulative energy curve and is in the elastic phase of the water-bearing sandstone specimen. The key point "B" is the inflection point where the energy growth rate begins to decrease and is in the unsteady crack propagation phase of the water-bearing sandstone specimen. The key point "C" is corresponding to the peak stress point of the water-bearing sandstone specimen.

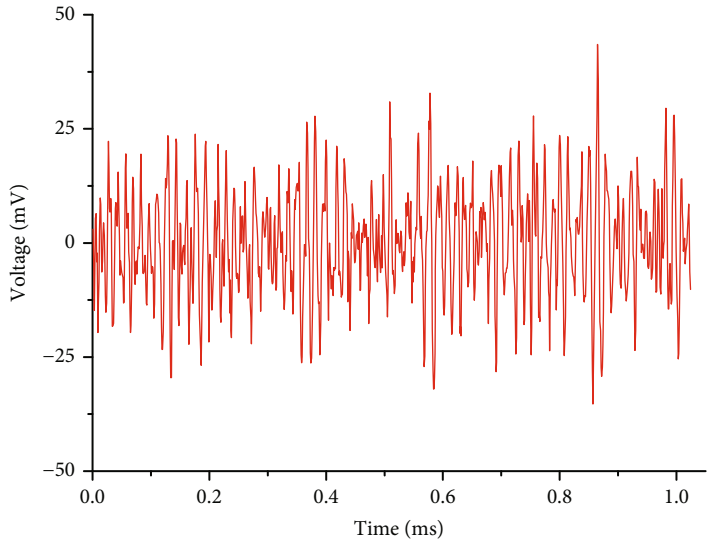

(a) Denoised signal

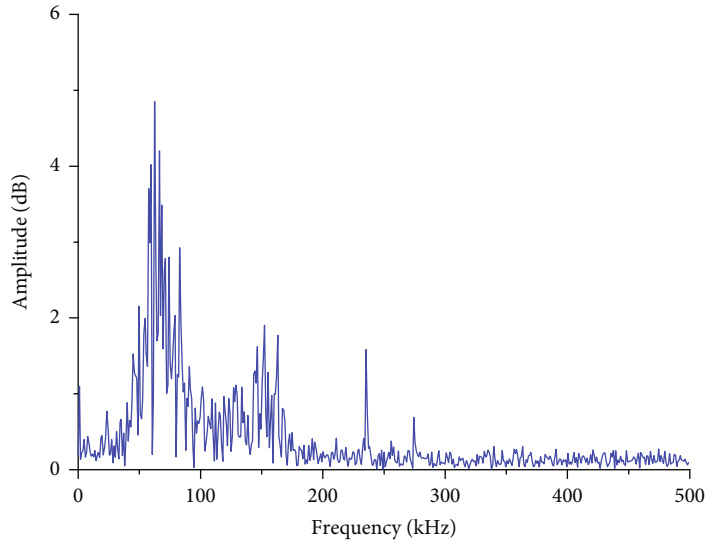

(b) Two-dimensional frequency spectrum

Figure 10: Denoised signals and two-dimensional frequency spectrum near key point "C.".

3.2.2. Dominant Frequency Characteristics near Key Points. As a nonstationary signal, it is difficult for AE signals to reflect all characteristics in the time domain. FFT needs to be used to analyze the signals in the frequency domain. FFT can decompose the time domain waveform signal into the superposition of sine wave signals with different frequencies and amplitudes to obtain the frequencies of these sine wave signals. This method can convert the signal information from the time domain to the frequency domain, and its principle is as follows:

$$X(\omega) = \int_{-\infty}^{+\infty} x(t) e^{-j\omega t} \mathrm{d}t, \tag{4}$$

where $X(\omega)$ is the expression of the original signal in the frequency domain and $x(t)$ is the expression of the original signal in the time domain.

Because AE signals are affected by the surrounding environment in the data acquisition process, it is inevitable to mix some noises. Therefore, firstly, the AE waveform signals should be denoised. The mixed threshold rule of Heursure, soft threshold function, and Daubechies wavelet basis are chosen for AE signal denoising. The denoised signals near three key points and the two-dimensional frequency spectrum obtained by FFT are shown in Figures 8, 9, and 10.

From Figure 8(b), the dominant frequency near the key point "A" is 60.55 kHz, and the two-dimensional frequency spectrum of AE waveform signals shows a bimodal structure. From Figure 9(b), the dominant frequency near the key point "B" is 58.59 kHz, and the two-dimensional frequency spectrum of AE waveform signals shows a three-peak structure. From Figure 10(b), the dominant frequency near the key point "C" is 62.50 kHz, and the two-dimensional frequency spectrum of AE waveform signals shows a three-peak structure. The above data shows that the dominant frequency of the water-bearing

Table 3: Energy proportion in each frequency band near three key points.

Frequency band number	Frequency band range (kHz)	Energy proportion (%)		
		Key point "A"	Key point "B"	Key point "C"
1	0~62.5	33.9	22.12	22.54
2	62.5~125	46.02	50.23	56.41
3	125~187.5	15.89	23.3	16.48
4	187.5~250	2.34	1.93	2.08
5	250~312.5	0.44	0.39	0.48
6	312.5~375	0.57	1.35	0.84
7	375~437.5	0.35	0.35	0.6
8	437.5~500	0.49	0.33	0.57

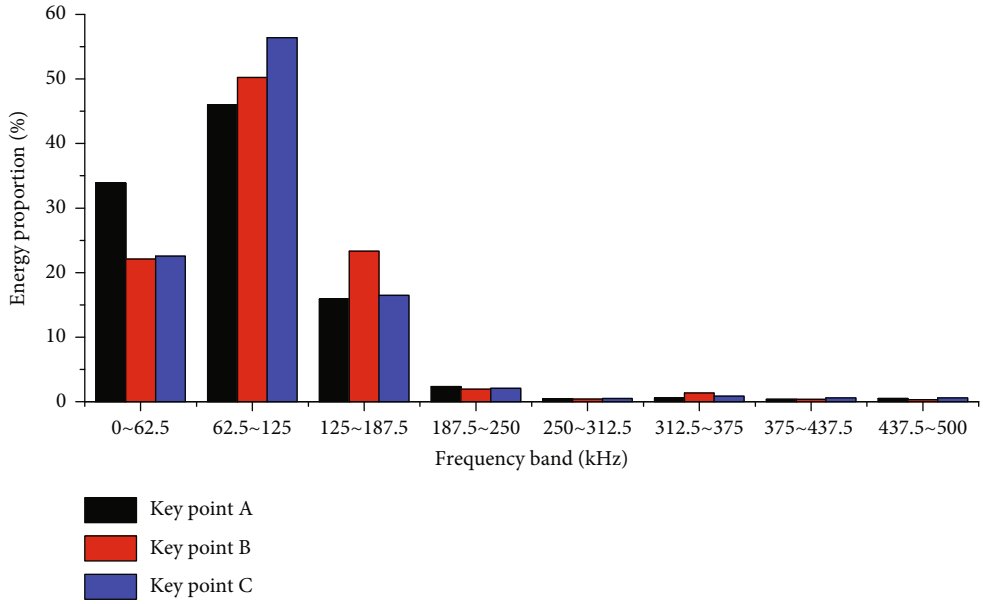

Figure 11: Energy proportion in each frequency band near three key points.

sandstone specimen is the highest at the peak stress point, followed by the elastic phase, and the minimum at the unsteady crack propagation phase. The current research shows that the different dominant frequencies is corresponding to different-sized crack propagation. The high frequency indicates that small-sized cracks are generated, and the low frequency is corresponding to the formation of large-sized cracks [24]. However, the difference of the dominant frequency among the three key points is very small, indicating that the crack initiation and propagation of the water-bearing sandstone specimen have a certain stability in the damage and failure process. This shows that the water has an influence on the failure mode of the sandstone specimen. Besides, the two-dimensional frequency spectrum structure of AE waveform signals shows that the failure mode of the water-bearing sandstone specimen near the key points "B" and "C" is more complex than that near the key point "A." That is, the closer to failure, the specimen produces more failure modes. So, the failure of the water-bearing sandstone specimen can be predicted by the number of multi-peak structures in the two-dimensional frequency spectrum. In general, the closer to failure, the more the number of peaks.

3.2.3. Wavelet Packet Analysis of AE Signal. Different-sized cracks release different amounts of energy in the process of specimen compression failure. So, the wavelet packet analysis method is used to decompose the AE waveform signals, which is helpful to understand the energy distribution characteristics of AE signals in different frequency bands. The wavelet packet can simultaneously decompose the high-frequency and low-frequency parts of the signals, which improves the time-frequency resolution of AE signals. In this paper, the Meyer wavelet is employed to decompose the AE waveform signals near three key points by three layers; that is, it is decomposed into eight frequency bands. The energy distribution characteristics of each frequency band near the three key points are shown in Table 3 and Figure 11.

From Table 3 and Figure 11, near the key points "A," "B," and "C," the total energy proportions of the first three frequency bands are 95.81%, 95.65%, and 95.43%, respectively. Among them, the energy of the no. 2 frequency band accounts for the highest and is 46.02%, 50.23%, and 56.41%, respectively. It is the dominant energy frequency band of the

AE signals, which determines the main failure mode of the water-bearing sandstone specimen. In the no. 4~no. 8 frequency bands, the total energy proportions are 4.19%, 4.35%, and 4.57%, respectively. In the latter five frequency bands, the energy proportion of each frequency band does not exceed 3%, which has little effect on the failure of the water-bearing sandstone specimen. The above analysis shows that the energy of AE signals is mainly concentrated in the first three frequency bands. But, the closer to failure, the more the energy proportion of the first three frequency bands is reduced; conversely, the energy proportion of the latter five frequency bands is increased, which leads to more complexity of the failure modes of the water-bearing sandstone specimen. This characteristic can be used as a precursor to predict the failure and instability of the water-bearing sandstone specimen.

4. Conclusions

In this paper, the AE characteristic parameters, dominant frequency, and frequency band energy evolution characteristics of the water-bearing sandstone specimen are studied by time domain and frequency domain analysis methods. The main conclusions are presented as follows:

(1) The violent fluctuation of AE time domain parameters indicates that the water-bearing sandstone specimen is about to be destroyed. This characteristic provides a theoretical basis for predicting the failure of the water-bearing rock in engineering practice

(2) The AE b value fluctuates during the uniaxial compression process. In the elastic phase, the AE b value is the lowest, but the AE b value has a sudden increase after falling into the steady crack growth phase. In the unsteady crack growth phase, the AE b value is further increased. This characteristic is of great indicative value for predicting the failure of the water-bearing sandstone specimen

(3) The difference of the dominant frequency among the three key points is very small, indicating that the crack initiation and propagation of the water-bearing sandstone specimen has a certain stability in the damage and failure process. But, the two-dimensional frequency spectrum structure of AE waveform signals shows that the closer to failure, the more the number of the frequency spectrum structure peaks

(4) The energy of AE signals is mainly concentrated in the first three frequency bands. The closer to failure, the more the energy proportion of the first three frequency bands is reduced; conversely, the energy proportion of the latter five frequency bands is increased, which leads to more complexity of the failure modes of the water-bearing sandstone specimen

Data Availability

All relevant data used to support the findings of this study are included within the article and also available from the corresponding author upon request.

Conflicts of Interest

The authors declare that they have no conflicts of interest.

Acknowledgments

This research was supported by the Natural Science Foundation of Inner Mongolia (Grant No. 2021BS05002) and the Natural Science Innovation Foundation of Inner Mongolia University of Science and Technology (Grant No. 2019QDL-B25).

References

[1] Y. J. Yang, N. N. Zhao, D. P. Ma, and F. J. Zhang, "Study on stability of strip coal pillar with different moisture content," *Journal of Mining & Safety Engineering*, vol. 33, no. 1, pp. 42–48, 2016.

[2] X. L. Li, Z. Y. Cao, and Y. L. Xu, "Characteristics and trends of coal mine safety development," *Energy Sources, Part A: Recovery, Utilization, and Environmental Effects*, no. 12, pp. 1–19, 2020.

[3] D. P. Ma, *Basic experiment research of failure mechanism and precursory characteristics of rock under triaxial unloading confining pressure [Ph.D. thesis]*, Shandong University of Science and Technology, China, 2016.

[4] T. B. Zhao, M. L. Xing, W. Y. Guo, C. W. Wang, and B. Wang, "Anchoring effect and energy-absorbing support mechanism of large deformation bolt," *Journal of Central South University*, vol. 28, no. 2, pp. 572–581, 2021.

[5] E. Aker, D. Kühn, V. Vavryčuk, M. Soldal, and V. Oye, "Experimental investigation of acoustic emissions and their moment tensors in rock during failure," *International Journal of Rock Mechanics and Mining Sciences*, vol. 70, no. 3, pp. 286–295, 2014.

[6] E. J. Kaiser, *A study of acoustic phenomena in tensile test [Ph.D. Thesis]*, Technische Hochschule München, Munich, Germany, 1959.

[7] Q. B. Meng, M. W. Zhang, L. J. Han, H. Pu, and T. Y. Nie, "Effects of acoustic emission and energy evolution of rock specimens under the uniaxial cyclic loading and unloading compression," *Rock Mechanics and Rock Engineering*, vol. 49, no. 10, pp. 3873–3886, 2016.

[8] M. W. Zhang, Q. B. Meng, S. D. Liu, D. Y. Qian, and N. Zhang, "Impacts of cyclic loading and unloading rates on acoustic emission evolution and felicity effect of instable rock mass," *Advances in Materials Science & Engineering*, vol. 2018, article 8365396, p. 16, 2018.

[9] X. L. Li, S. J. Chen, E. Y. Wang, and Z. H. Li, "Rockburst mechanism in coal rock with structural surface and the microseismic (MS) and electromagnetic radiation (EMR) response," *Engineering Failure Analysis*, vol. 124, article 105396, no. 6, p. 14, 2021.

[10] L. R. Li, J. H. Deng, L. Zheng, and J. F. Liu, "Dominant frequency characteristics of acoustic emissions in white marble

during direct tensile tests," *Rock Mechanics and Rock Engineering*, vol. 50, no. 5, pp. 1337–1346, 2017.

[11] J. P. Liu, Y. H. Li, S. D. Xu, S. Xu, C. Y. Jin, and Z. S. Liu, "Moment tensor analysis of acoustic emission for cracking mechanisms in rock with a pre-cut circular hole under uniaxial compression," *Engineering Fracture Mechanics*, vol. 135, pp. 206–218, 2015.

[12] Z. Moradian, H. H. Einstein, and G. Ballivy, "Detection of cracking levels in brittle rocks by parametric analysis of the acoustic emission signals," *Rock Mechanics and Rock Engineering*, vol. 49, no. 3, pp. 785–800, 2016.

[13] C. Y. Wang, X. K. Chang, Y. L. Liu, and S. J. Chen, "Mechanistic characteristics of double dominant frequencies of acoustic emission signals in the entire fracture process of fine sandstone," *Energies*, vol. 12, no. 20, article 3959, p. 17, 2019.

[14] J. Zhang, W. H. Peng, F. Y. Liu, H. X. Zhang, and Z. J. Li, "Monitoring rock failure processes using the Hilbert-Huang transform of acoustic emission signals," *Rock Mechanics and Rock Engineering*, vol. 49, no. 2, pp. 427–442, 2016.

[15] C. Y. Wang, X. K. Chang, and X. Y. Du, "Analysis on dominant-frequency characteristics of acoustic emission in sandstone uniaxial compression failure," *Chinese Journal of Underground Space and Engineering*, vol. 16, no. 2, pp. 451–462, 2020.

[16] C. Y. Wang, X. K. Chang, Y. L. Liu, and W. B. Guo, "Spectrum evolution characteristics of acoustic emission during the rupture process of marble under uniaxial compression condition," *Rock and Soil Mechanics*, vol. 41, no. 1, pp. 51–62, 2020.

[17] X. L. Li, S. J. Chen, S. M. Liu, and Z. H. Li, "AE waveform characteristics of rock mass under uniaxial loading based on Hilbert-Huang transform," *Journal of Central South University*, vol. 28, no. 6, pp. 1843–1856, 2021.

[18] K. Du, X. F. Li, M. Tao, and S. F. Wang, "Experimental study on acoustic emission (AE) characteristics and crack classification during rock fracture in several basic lab tests," *International Journal of Rock Mechanics and Mining Sciences*, vol. 133, article 104411, p. 15, 2020.

[19] M. Sheng, S. C. Tian, B. Zhang, and H. K. Ge, "Frequency analysis of multi-sources acoustic emission from high-velocity waterjet rock drilling and its indicator to drilling efficiency," *International Journal of Rock Mechanics and Mining Science*, vol. 115, pp. 137–144, 2019.

[20] F. D. Mei, C. Y. Hu, P. Y. Li, and J. S. Zhang, "Study on main frequency precursor characteristics of acoustic emission from deep buried Dali rock explosion," *Arabian Journal of Geosciences*, vol. 12, no. 21, article 645, p. 12, 2019.

[21] P. Zeng, Y. J. Liu, H. G. Ji, and C. J. Li, "Coupling criteria and precursor identification characteristics of multi-band acoustic emission of gritstone fracture under uniaxial compression," *Chinese Journal of Geotechnical Engineering*, vol. 39, no. 3, pp. 509–517, 2017.

[22] M. C. He, F. Zhao, Y. Zhang, S. Du, and L. Guan, "Feature evolution of dominant frequency components in acoustic emissions of instantaneous strain-type granitic rockburst simulation tests," *Rock and Soil Mechanics*, vol. 36, no. 1, pp. 1–8+33, 2015.

[23] B. Fu, Z. H. Zhou, H. Q. Wang, and Y. X. Wang, "Precursor information study on acoustic emission characteristics of marble under uniaxial cyclic loading-unloading," *Journal of China Coal Society*, vol. 41, no. 8, pp. 1946–1953, 2016.

[24] M. Cai, P. K. Kaiser, H. Morioka et al., "FLAC/PFC coupled numerical simulation of AE in large-scale underground excavations," *International Journal of Rock Mechanics and Mining Sciences*, vol. 44, no. 4, pp. 550–564, 2007.